Journal of X-Ray Science and Technology 23 (2015) 791–797
DOI 10.3233/XST-150520
IOS Press

Brief Report

A laser driven pulsed X-ray backscatter technique for enhanced penetrative imaging

R.M. Deas[a], L.A. Wilson[b,*], D. Rusby[c], A. Alejo[d], R. Allott[b], P.P. Black[a], S.E. Black[a], M. Borghesi[d], C.M. Brenner[b], J. Bryant[e], R.J. Clarke[b], J.C. Collier[b], B. Edwards[f], P. Foster[b], J. Greenhalgh[b], C. Hernandez-Gomez[b], S. Kar[d], D. Lockley[a], R.M. Moss[a,g], Z. Najmudin[e], R. Pattathil[b], D. Symes[b], M.D. Whittle[a], J.C. Wood[e], P. McKenna[c] and D. Neely[b,c]
[a]*Security Sciences Department, DSTL, Fort Halstead, Sevenoaks, Kent, UK*
[b]*Central Laser Facility, STFC Rutherford Appleton Laboratory, Chilton, Didcot, UK*
[c]*SUPA Department of Physics, University of Strathclyde, Glasgow, UK*
[d]*Department of Physics and Astronomy, Queens University of Belfast, Belfast, UK*
[e]*Blackett Laboratory, Imperial College London, London, UK*
[f]*Innovations, STFC, Rutherford Appleton Laboratory, Chilton, Didcot, UK*
[g]*Department of Medical Physics and Biomedical Engineering, University College London, London, UK*

Received 10 February 2015
Revised 20 July 2015
Accepted 21 August 2015

Abstract. X-ray backscatter imaging can be used for a wide range of imaging applications, in particular for industrial inspection and portal security. Currently, the application of this imaging technique to the detection of landmines is limited due to the surrounding sand or soil strongly attenuating the 10s to 100s of keV X-rays required for backscatter imaging. Here, we introduce a new approach involving a 140 MeV short-pulse (< 100 fs) electron beam generated by laser wakefield acceleration to probe the sample, which produces Bremsstrahlung X-rays within the sample enabling greater depths to be imaged. A variety of detector and scintillator configurations are examined, with the best time response seen from an absorptive coated BaF_2 scintillator with a bandpass filter to remove the slow scintillation emission components. An X-ray backscatter image of an array of different density and atomic number items is demonstrated. The use of a compact laser wakefield accelerator to generate the electron source, combined with the rapid development of more compact, efficient and higher repetition rate high power laser systems will make this system feasible for applications in the field.

Keywords: X-ray backscatter, X-ray radar, X-ray imaging systems, X-ray, detection

*Corresponding author: L.A. Wilson, Central Laser Facility, STFC Rutherford Appleton Laboratory, Chilton, Didcot, OX11 0QX, UK. E-mail: lucy.wilson@stfc.ac.uk.

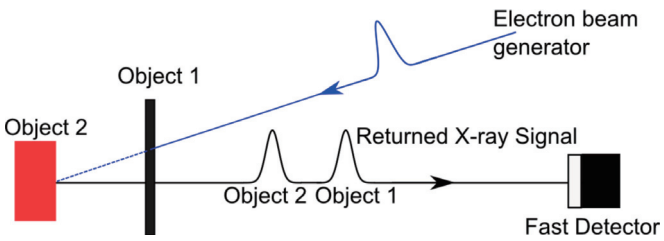

Fig. 1. Schematic of electron generated X-ray backscatter detection. (Colours are visible in the online version of the article; http://dx.doi.org/10.3233/XST-150520)

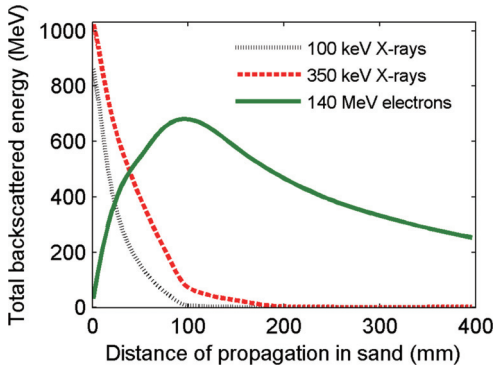

Fig. 2. A comparison of the total backscattered X-ray energy as a function of depth from 100 keV X-rays (black dotted line), 350 keV X-rays (red dashed line) and 140 MeV electrons (solid green line) as a function of areal density for a sand target. The simulation is performed using the Geant4 model [7,8]. (Colours are visible in the online version of the article; http://dx.doi.org/10.3233/XST-150520)

1. Introduction

X-ray backscatter imaging is currently used for a range of imaging applications in particular for portal security where it is used to scan shipping containers, vehicles and people [1,2]. It has the advantage over transmissive X-ray imaging of having the detector and X-ray source on the same side of the sample allowing for single sided imaging. X-ray backscatter imaging also shows an increased sensitivity to lower atomic number materials compared to X-ray transmission imaging and has the potential to distinguish between materials based on their atomic number and density which has applications for explosive screening [3].

Inelastic or Compton scattering of X-rays tends to be the dominant mechanism for the attenuation of X-rays from a few 10s of keV–10s of MeV (dependant on the atomic number of the material). X-rays are preferentially scattered in the forward direction with lower X-ray energies having the largest backwards scattered component (from the Klein-Nishina formula [4]). Attempts to apply X-ray backscatter imaging technology to the detection of landmines have encountered difficulties due to the 10s–100s of keV X-rays required for a strong backscattered signal being highly attenuated by sand and soil at these energies. Work by Dugan et al. [5] shows backscatter images of landmines at a maximum depth of 50 mm beneath soil and grass using an X-ray tube source with a maximum photon energy of 160 keV. At more than 50 mm depth the attenuation and scattering of the X-rays becomes too large to allow good imaging. The use of higher energy, 350 keV and 1 MeV X-rays have been examined in Monte-Carlo simulations performed by Heuvel et al. [6] and are shown to be able to image down to greater depths, with imaging at 70 mm below the soil calculated to be possible despite the reduction in the proportion of backscattered X-rays. However, the number of multiple scattering events increases as the energy increases reducing the potential horizontal resolution of the image.

High energy electrons are able to penetrate to greater depths in a sample and to be tuned to produce a peak in backscatter emission at a particular depth. Electrons produce X-rays in the sample via bremsstrahlung emission. The X-rays produced then backscatter and are attenuated as they travel back through the sample. An example of how this scheme works is shown in Fig. 1. The interaction between

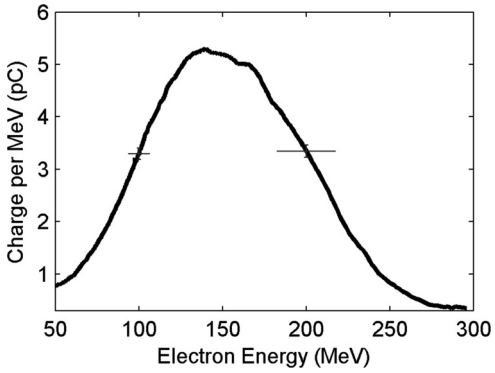

Fig. 3. Electron spectrum measured on a Kodak Lanex screen. Electrons are produced with 3.9×10^{18} cm^{-3} He + 5% N_2 gas jet and deflected by a 100 mm 0.67 T magnet. Peak energy is shown to be approximately 140 MeV ± 10 MeV with a 120 MeV FWHM energy spread. Typical error bars for points at either end of the spectrum are shown. These errors are largely due to uncertainties in position measurements and the charge calibration.

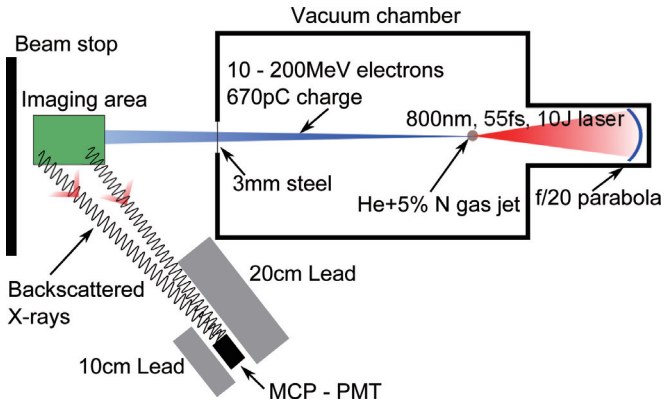

Fig. 4. Plan view diagram of experimental set-up showing positions of MCP-PMT detectors, imaging samples, gas jet and electron beam. (Colours are visible in the online version of the article; http://dx.doi.org/10.3233/XST-150520)

these effects leads to the peak in backscatter emission shown in Fig. 2. X-ray beams, however, are attenuated as they enter and are backscattered in the sample. This is demonstrated in Fig. 2 which shows the results of simulations using Geant4 [7,8] to simulate the total backscattered X-ray energy per unit length from sand (SiO_2 with a density of 1.78 gcm^{-3}) as a function of distance when probed with 350 keV X-rays, 100 keV X-rays and 140 MeV electrons. The simulation was conducted with 10^6 incident electrons. The backscattered X-ray flux was measured using a detector plane on the front surface of the sand sample. In this letter we demonstrate a new approach using a laser generated 140 MeV electron beam as the radiation source. As the electrons are slowed down in the imaging target they emit bremsstrahlung X-rays which are then backscattered and detected. This is the first time such an imaging technique has been demonstrated.

2. Method

The experiment was performed using the Gemini dual beam Ti:Sapphire 800 nm laser system at the Central Laser Facility at the Rutherford-Appleton Laboratory [9]. The Gemini laser is able to produce pulses of 55 ± 5 fs duration and energies of 10 ± 1 J on target. A single p-polarised beam of Gemini was focused into the centre of a supersonic gas jet at normal incidence using an $f/20$ off-axis parabolic mirror. The focal spot Full Width Half Maximum (FWHM) was measured to be 25 μm, resulting in a peak intensity of 10^{19} Wcm^{-2}.

Gemini is capable of producing narrow energy spread electron beams of up to GeV energies [10]. To provide optimal conditions for the production of a high flux of detectable backscattered X-rays from a sample, highly reproducible electron beams are required with lower electron energies typically between 10–200 MeV. This increases the fraction of lower energy X-rays (10s to 100s of keVs) that are most likely to be backscattered. A high charge beam is also required to increase the backscattered signal as the X-ray backscatter signal is much lower than the forward scattered beam. To achieve this, an $f/20$

focusing optic was used to provide a large focal spot within a supersonic gas jet ($\approx 25\ \mu$m). This enables the creation of a larger non-linear plasma wave bubble within the gas, increasing the limit on the number of electrons that can be injected. A 5 mm gas jet nozzle was used with the laser focused 1 mm above the tip of the nozzle. A helium and 5% nitrogen gas mix was used allowing for ionisation injection to occur – previously shown to lead to an increase in the total charge in the electron beam [11,12].

To characterise the generated electron beam, electron spectra were measured by placing a 0.67 T 100 mm long magnet on-axis to deflect the electron beam though a 1 mm Al window onto a scintillation screen (Kodak Lanex, emission peak at 546 nm) at the end of the chamber 1.83 m from the gas jet. This was imaged on to a 16 bit CCD camera to obtain the electron spectrum. A scan of gas electron densities up to 5×10^{18} cm^{-3} was performed which showed the most consistent, high flux and uniform electron beams in the 50–300 MeV region at a gas electron density of 3.9×10^{18} cm^{-3} $\pm$ 0.1×10^{18} cm^{-3} (A sample of an electron spectrum at 3.9×10^{18} cm^{-3} is shown in Fig. 3). The total electron beam charge – calibrated by placing image plate in the beam path (image plate counts can be converted to PSL [13], where 1 PSL $\approx$ 50 electrons for image plate type BAS-MS in this energy range [14]), is found to be 670 pC $\pm$ 30 pC from an average of 30 shots. The vertical divergence of the electron beam was typically 6.0 mrads $\pm$ 1.2 mrads, measured over 16 shots.

To scan an array of objects, the magnet was removed and the electron beam propagated out of the vacuum chamber through a 3 mm thick steel window on the laser axis 1.8 m from the gas jet. A layout of the experiment is shown in Fig. 4. Samples to be scanned were typically placed between 0.4 m–1.5 m from the end of the vacuum chamber (2.2 m–3.3 m from the gas jet). Behind the samples, 2.25 m from the end port there is a 0.3 m thick lead electron beam stop which gives a strong X-ray backscatter signal. It is possible to shield the detectors from this signal using a lead collimator, however, it could also be used as a reference X-ray scatter point. Micro Channel Plate Photomultiplier Tube (MCP-PMT) detectors [15] were placed $\approx$ 2.2 m away from the sample within lead shielding to restrict the field of view and suppress unwanted background X-ray emission associated with electrons interacting with the vacuum chamber walls.

Initial tests of the MCP-PMT response were carried out to study the time resolution of the detectors with different scintillator materials and geometries. Three different scintillator set-ups were tested: (1) BC422Q plastic scintillator with 0.5% benzophenone doping in a 50 mm long 50 mm diameter cylinder with a reflective coating, (2) 10 mm $\times$ 10 mm $\times$ 80 mm BC422Q 0.5% cuboid with a absorptive coating, and (3) an array of 4 $\times$ 10 mm $\times$ 10 mm $\times$ 10 mm BaF_2 crystals with a 195 nm bandpass filter to remove the slower 220 nm component of the scintillator emission. Both BC422Q and BaF are expected to have a similar characteristic decay time of 600 ps–800 ps. The MCP-PMT window diameter is 11 mm. The MCP-PMTs with the plastic BC422Q scintillator were placed with the entire scintillator vertically in the electron beam to enable direct comparison. The BaF_2 scintillator response is to the backscattered X-ray signal from 38 mm of Al.

The response curves are shown in Fig. 5. The BaF_2 response is scaled up by a factor of 5 to enable comparison with other signals. The FWHM for scintillators (1), (2) and (3) are 3350 ps $\pm$ 54 ps, 1510 ps $\pm$ 41 ps and 710 ps $\pm$ 25 ps respectively. This shows an increase in resolution with a thinner absorptive coated scintillator due to the reduction of the number of different possible path lengths for detected light. The best resolution found was with the 10 mm $\times$ 10 mm $\times$ 10 mm BaF_2. This is due to the decrease in length of scintillator required for a given stopping power due to the higher density of BaF_2 compared to BC422Q. The BaF_2 response appears be to associated with a decrease in the signal amplitude. This is due to the weaker emission from the fast 195 nm decay as well as the signal being from a backscatter target rather than direct beam irradiation as for the plastic scintillators. This was alleviated by taking multiple shots on a target and summing the resulting responses over 20–40 shots to improve the signal to noise ratio.

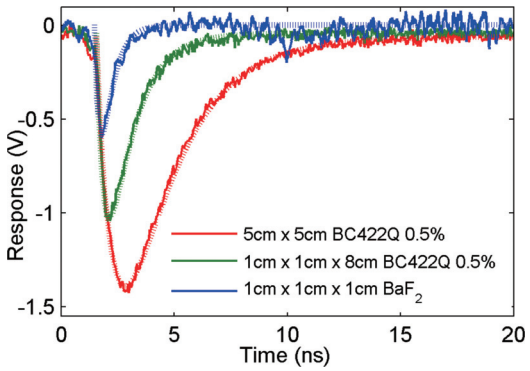

Fig. 5. Comparison of output signal from BC422Q 0.5% plastic scintillators in a 50 mm long 50 mm diameter cylinder (red line), 10 mm × 10 mm × 80 mm cuboid (green line) and 4 10 mm × 10 mm × 10 mm BaF_2 crystals (blue line) with a 195 nm bandpass filter. Data is averaged over 4, 5 and 10 shots respectively and the BaF_2 signal has been scaled up by a factor of 5 to allow comparison with the other signals. Dashed lines show curve fits assuming curve of the form $\exp(-t/t_{decay}) - \exp(-t/t_{rise})$ [16], where t_{decay} and t_{rise} are the decay and rise time constants. (Colours are visible in the online version of the article; http://dx.doi.org/10.3233/XST-150520)

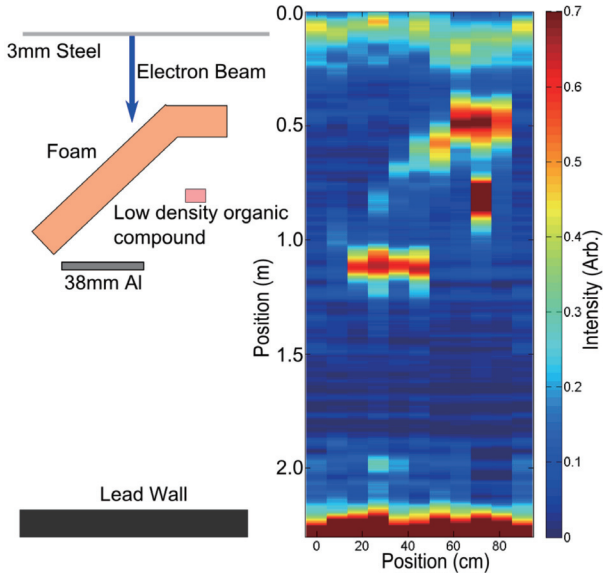

Fig. 6. (a) Diagram of the set-up of the array of test objects. (b) Example of an X-ray backscatter image of the object array shown in (a). An array of objects including 38 mm thick Al, 0.14 m thick insulation foam and a low density organic compound are shown. (Colours are visible in the online version of the article; http://dx. doi.org/10.3233/XST-150520)

3. Results and discussion

An array of objects chosen to give a variety of mass densities and atomic numbers including 0.14 m thick foam wall insulation, 38 mm thick aluminium and a 0.10 m × 0.05 m × 0.15 m bag of low density organic compound ($C_{12}H_{22}O_{11}$) were set up as shown in Fig. 6(a). The detectors are to the side of the vacuum chamber 2.2 m from the 38 mm Al as shown in Fig. 4. Each x axis 'slice' of the resulting 'X-ray radar' image shown in Fig. 6(b) corresponds to a 0.1 m horizontal displacement of the object with respect to the beam. The resolution in the y axis is dependent on the combined scintillator and detector time response. Each slice is an average of the BaF_2 MCP-PMT signal over 40 shots. The zero position is given as the signal from the 3 mm steel window, with distances (in m) given from this position, with the lead beam stop shown at 2.20 m. The X-ray radar image clearly shows positions of the different density and atomic number objects shown in Fig. 6, with the objects positioned behind the 0.14 m foam 'wall' being observed to have a strong response demonstrating the potential for single sided imaging of objects behind a barrier. This is due to 140 MeV electrons having a much greater penetration depth than the 10 s to 100 s of keV X-rays required for backscatter detection. These electrons are able to pass through the foam wall and generate X-rays within the sample which then backscatter and pass back through the foam wall to the detector, direct X-ray irradiation would require the X-rays to pass through the foam wall twice being attenuated both times and giving a weaker signal from the sample behind the wall.

4. Conclusions

A 140 MeV electron beam generated by laser wakefield acceleration has been propagated in air and

used to induce an X-ray backscatter image of an array of objects. This represents the first demonstration of such an image. The use of a laser wakefield generated electron beam has the advantage of producing electrons of high intensity and energy in an ultra-short time scale from a very compact accelerator. Ultra-high peak power laser technology is developing rapidly with pulse repetition rates and efficiency increasing whilst system size is reduced [17]. These rapid developments in laser technology make it possible to envisage fielding this type of accelerator and detector system for inspection in the field in the near future. The shortest time resolution and, therefore, depth resolution was found with an MCP-PMT with an absorptive coated 10 mm $\times$ 10 mm $\times$ 10 mm BaF_2 scintillator using a bandpass filter at 195 nm to absorb the slower emission at 220 nm and transmit the fast emission. This method has the potential to image at greater depths than previously demonstrated with X-ray source imaging techniques due to the greater propagation range of electrons compared with X-rays. The authors believe the image quality is limited by the emittance of the electron beam and the temporal response of the X-ray detectors as the pulse length of the laser driven electrons can achieve a depth resolution of 0.3 mm. Signal to noise ratio of the X-ray backscatter signal can be enhanced by a higher electron beam charge, an increased pulse repetition rate or a larger area X-ray detector.

Acknowledgements

This work was supported by funding from MoD Science and Technology Programme and STFC Business and Innovations Directorate. The authors would like to thank the staff at the Central Laser Facility for their support. S. Kar would like to acknowledge support from EPSRC through grant EP/J002550/1. Data associated with research published in this paper can be accessed by contacting the corresponding author.

References

[1] A. Chalmers, Rapid inspection of cargos at portals using drive-through transmission and backscatter X-ray imaging, *Proceedings of SPIE* **5403** (September 2004), 644–648.
[2] A. Chalmers, Three applications of backscatter X-ray imaging technology to homeland defense, *Proceedings of SPIE* **5778** (May 2005), 989–993.
[3] C. Paulus, J. Tabary, N.B. Pierron, J.M. Dinten, E. Fabiani, F. Mathy, F. Mougel, J. Rinkel and L. Verger, A multi-energy X-ray backscatter system for explosives detection, *Journal of Instrumentation* **8**(4) (April 2013), P04003–P04003.
[4] O. Klein and Y. Nishina, ber die streuung von strahlung durch freie elektronen nach der neuen relativistischen quantendynamik von dirac, *Zeitschrift fr Physik* **52**(11–12) (1929), 853–868.
[5] E.T. Dugan, A.M. Jacobs, Z. Su, L. Houssay, D. Ekdahl and S. Brygoo, Development and field testing of a mobile backscatter X-ray lateral migration radiography land mine detection system, *Proceedings of SPIE* **4742** (August 2012), 120–131.
[6] J. van den Heuvel and F. Fiore, Simulation study of X-ray backscatter imaging of pressure-plate improvised explosive devices, *Proc SPIE* **8357** (2012), 835716-835716-15.
[7] J. Allison, K. Amako, J. Apostolakis, H. Araujo, P.A Dubois, M. Asai, G. Barrand, R. Capra, S. Chauvie, R. Chytracek, G.A.P. Cirrone, G. Cooperman, G. Cosmo, G. Cuttone, G.G. Daquino et al., Geant4 developments and applications, *Nuclear Science, IEEE Transactions on* **53**(1) (Feb 2006), 270–278.
[8] S. Agostinelli, J. Allison, K. Amako, J. Apostolakis, H. Araujo, P. Arce, M. Asai, D. Axen, S. Banerjee, G. Barrand, F. Behner, L. Bellagamba, J. Boudreau, L. Broglia, A. Brunengo et al., Geant4a simulation toolkit, *Nuclear Instruments and Methods in Physics Research Section A: Accelerators, Spectrometers, Detectors and Associated Equipment* **506**(3) (2003), 250–303.
[9] C.J. Hooker, J.L. Collier, O. Chekhlov, R. Clarke, E. Divall, K. Ertel, B. Fell, P. Foster, S. Hancock, A. Langley, D. Neely, J. Smith and B. Wyborn, The astra gemini project a dual-beam petawatt ti: Sapphire laser system, *J Phys IV France* **133** (2006), 673–677.

[10] S. Kneip, S. Nagel, S. Martins, S. Mangles, C. Bellei, O. Chekhlov, R. Clarke, N. Delerue, E. Divall, G. Doucas, K. Ertel, F. Fiuza, R. Fonseca, P. Foster, S. Hawkes, C. Hooker, K. Krushelnick, W. Mori, C. Palmer, K. Phuoc, P. Rajeev, J. Schreiber, M. Streeter, D. Urner, J. Vieira, L. Silva and Z. Najmudin, Near-gev acceleration of electrons by a nonlinear plasma wave driven by a self-guided laser pulse, *Physical Review Letters* **103**(3) (July 2009), 035002.
[11] C. McGuffey, A.G.R. Thomas, W. Schumaker, T. Matsuoka, V. Chvykov, F.J. Dollar, G. Kalintchenko, V. Yanovsky, A. Maksimchuk, K. Krushelnick, V.Yu. Bychenkov, I.V. Glazyrin and A.V. Karpeev, Ionization induced trapping in a laser wakefield accelerator, *Physical Review Letters* **104**(2) (January 2010), 025004.
[12] A. Pak, K.A. Marsh, S.F. Martins, W. Lu, W.B. Mori and C. Joshi, Injection and trapping of tunnel-ionized electrons into laser-produced wakes, *Physical Review Letters* **104**(2) (January 2010), 025003.
[13] I.J. Paterson, R.J. Clarke, N.C. Woolsey and G. Gregori, Image plate response for conditions relevant to laserplasma interaction experiments, *Measurement Science and Technology* **19**(9) (September 2008), 095301.
[14] S. Kneip, *Laser Plasma Accelerator and Wiggler*, PhD thesis, Imperial College, London, 2010.
[15] Hamamatsu Photonics K.K Editorial Committee, *Photomultiplier Tubes – Basics and applications*, chapter 10, Hamamatsu Photonics K.K Electron Tube Division, 3 edition, 2007, pp. 187–208.
[16] G.F. Knoll, *Radiation Detection and Measurement*, chapter 8, Wiley, 3 edition, 1999, p. 229.
[17] P.D. Mason, M. Fitton, A. Lintern, S. Banerjee, K. Ertel, T. Davenne, J. Hill, S.P. Blake, P.J. Philips, T.J. Butcher, J.M. Smith, M. De Vido, R.J.S. Greenhalgh, C. Hernandez-Gomez and J. Collier, Scalable design for a high energy cryogenic gas cooled diode pumped laser amplifier, *Applied Optics* **54**(13) (2015), 4227.